Nanoscale

ROYAL SOCIETY OF CHEMISTRY

COMMUNICATION

View Article Online
View Journal | View Issue

Cite this: *Nanoscale*, 2023, **15**, 10985

Received 5th April 2023,
Accepted 6th June 2023

DOI: 10.1039/d3nr01574b

rsc.li/nanoscale

Ammonia-assisted synthesis of low-crystalline FeCo hydroxides for efficient electrochemical overall water splitting†

Huijun Ren,‡[a] Changgen Cheng,‡[a] Peiqun Yin,*[b] Qing Qin *[c] and Lei Dai *[a]

Low-crystalline FeCo hydroxides were synthesized on a gram scale with the aid of ammonia, and they exhibited impressive catalytic activity for both the HER and OER. We utilized these catalysts to assemble a water splitting cell, which functions efficiently. The electrolytic cell can produce a consistent current density of 200 mA cm^{-2} for over 20 hours while operating at a voltage of 1.95 V.

Hydrogen is widely regarded as the most ideal fuel due to its potential to address environmental problems caused by fossil fuel consumption.[1–7] Currently, there are mainly two methods to produce hydrogen, including high-temperature reforming of hydrogen-containing chemicals[8] and photo-electrochemical reforming of water.[9–19] However, high-temperature reforming requires high temperatures, pressures, and catalyst consumption, making it unsustainable and environmentally unfriendly. Conversely, electrochemical methods can be conducted under ambient conditions, making them a promising approach for synthetic chemistry in the future.[20–22] By controlling the given voltage, chemical reactions that previously required high temperatures and pressures can now be achieved with ease. For instance, water splitting to produce hydrogen only requires a voltage of 1.23 V. This is in sharp contrast to the high-temperature reforming process, which needs a high temperature above 1000 degrees and a substantial amount of catalysts.[8,10]

In developing electrochemical methods, there are still technical obstacles that need to be addressed, such as the development of high-efficiency electrocatalysts.[23] A desirable electrocatalyst candidate should have a low synthetic cost, a stable structure and high catalytic performance. Although electrocatalysts such as Pt, Ru, and Ir are effective at producing hydrogen through water electrolysis, their widespread use is restricted due to their limited availability and poor catalytic durability.[5,24–27] Under alkaline conditions, transition metal (Fe, Co, and Ni) sulfides, oxides, phosphides, nitrides, and selenides have shown promising catalytic performance for the electrolysis of water to produce hydrogen,[6,28–34] with FeNi LDH being reported as the most excellent anode catalyst.[35] However, their high synthetic cost poses a great challenge for industrialization. The ideal electrocatalyst for industrialization should have a low synthetic cost with simple procedures, while only a few reports of such synthetic systems have been achieved.[23,31,36–43]

In this study, we utilized ammonia as a template to synthesize a series of transition metal hydroxides. This method requires no heating and only involves stirring at room temperature for 30 minutes, enabling the preparation of low-crystalline FeCo hydroxides (LC-FeCo) on a gram-scale (see the ESI†). Remarkably, these hydroxides exhibited a low overpotential of only 320 mV to achieve a current density of 200 mA cm^{-2} in the oxygen evolution Reaction. Furthermore, they demonstrated exceptional stability and durability at high operating current densities, with an output current density of over 350 mA cm^{-2} maintained for 22 hours of electrolysis at a potential of 1.62 V. Moreover, these hydroxides also displayed excellent hydrogen evolution performance, with a high current density of 200 mA cm^{-2} being achieved at a potential of −0.32 V. Based on their outstanding electrocatalytic activity for the anode and cathode in water splitting, an electrolytic cell was constructed using low-crystalline FeCo hydroxides as the catalyst. Under a working voltage of 2 V, the output current density was approximately 200 mA cm^{-2}, surpassing that of electrolytic cells based on commercial precious metal catalysts in terms of both catalytic stability and activity.

LC-FeCo is synthesized using an NH_3 auxiliary strategy by adding NH_3 to a mixed solution of $FeCl_3$ and $CoCl_2$ in a glass

[a]*Key Laboratory for Special Functional Materials of Ministry of Education, School of Materials Science and Engineering, Henan University, Kaifeng 475004, China. E-mail: dailei@henu.edu.cn*

[b]*Center of Biomedical Materials Research and Engineering, School of Biomedical Engineering, Anhui Medical University, Hefei, 230032, China. E-mail: pqyin@mail.ustc.edu.cn*

[c]*Key Laboratory of Functional Molecular Solids, Ministry of Education, College of Chemistry and Materials Science, Anhui Normal University, Wuhu 241002, China. E-mail: qing.qin@ahnu.edu.cn*

†Electronic supplementary information (ESI) available. See DOI: https://doi.org/10.1039/d3nr01574b

‡These authors contributed equally to this work.

beaker and then stirring at room temperature for 30 minutes. This method has been used to synthesize various transition metal-based hydroxides. Layered LC-FeCo is obtained in high yield which is confirmed by the dark-field scanning transmission electron microscopy (STEM) and transmission electron microscopy (TEM) images (Fig. 1a and b). High-resolution transmission electron microscopy (HRTEM) images (Fig. 1c) reveal the presence of many holes and amorphous structures (Fig. 1d) on the hydroxide surface, indicating the existence of numerous defective sites. In a representative crystalline region (Fig. 1c and e), the crystal lattice with a lattice spacing of 2.43 Å is observed, corresponding to the (111) plane of hydroxide. The absence of diffraction peaks in the X-ray diffraction (XRD) pattern indicates the low-crystalline nature of the material (Fig. S1†). The appearance of a diffraction peak at 10–20° in the XRD pattern further confirms the layered structure characteristic of LC-FeCo, while the absence of diffraction peaks at 30–70° indicates the low-crystalline nature of the material (Fig. S1†). Elemental mappings (Fig. 1f) show a homogeneous distribution of Fe and Co in LC-FeCo, with an estimated Fe : Co atomic ratio of 3 : 5 obtained by inductively coupled plasma mass spectrometry (ICP-MS) and energy dispersive X-ray spectroscopy (EDX) (Fig. S2a†). It is particularly important that in the laboratory, we can achieve gram-level production of LC-FeCo without any heating treatment (Fig. S3†). So far, the low-crystalline FeCo catalyst has been prepared at room temperature by simple stirring, as illustrated in Scheme 1. Upon subjecting the obtained low-crystalline product to secondary heating treatment, the material underwent a transformation from its low-crystalline state to a high-crystalline state.

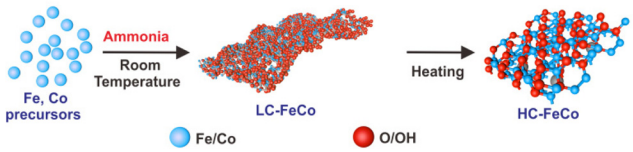

Scheme 1 Schematic illustration of the preparation of LC-FeCo and HC-FeCo catalysts.

As depicted in Fig. 2a and b, the high-crystalline FeCo hydroxides (HC-FeCo) obtained were observed to be formed by aggregated nanoparticles of approximately 5 nm in size. This suggests that layered LC-FeCo undergoes atomic restructuring upon secondary heating. From the HRTEM image (Fig. 2c–e), the atomic arrangement becomes clear, but the lattice spacing of 2.43 Å did not change significantly. Meanwhile, EDX mapping (Fig. 2f) shows that Fe and O elements are still evenly distributed, and the atomic ratio of FeCo remains at 3.3 : 4.7 (Fig. S2b†). Furthermore, the formation of a crystalline FeCo material after heat treatment is confirmed by the appearance of distinct diffrac-

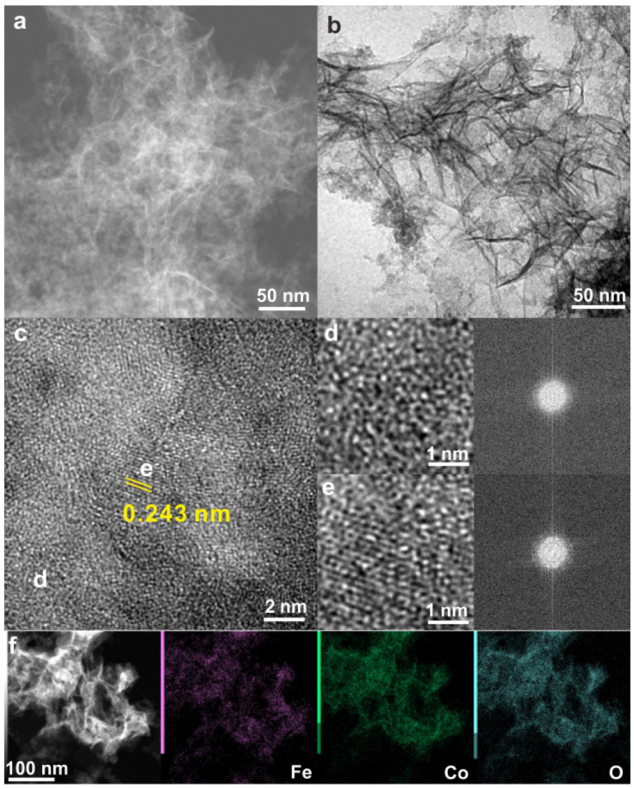

Fig. 1 TEM characterization of low-crystalline FeCo hydroxides. (a) STEM image, (b) TEM image, (c–e) HR-TEM images, and (f) EDX elemental mapping images.

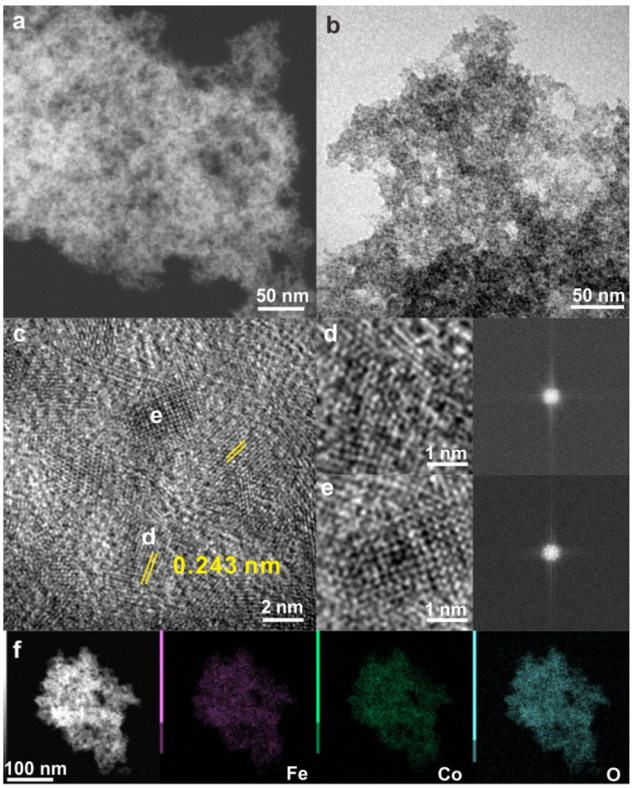

Fig. 2 TEM characterization of high-crystalline FeCo hydroxides. (a) STEM image, (b) TEM image, (c–e) HR-TEM images, and (f) EDX elemental mapping images.

tion peaks between 35 and 70°, while the weakening of the diffraction peak intensity at 10–20° indicates the disruption of its layered structure, as shown in the XRD pattern (Fig. S1†). This result is consistent with the TEM results.

We simultaneously used X-ray photoelectron spectroscopy (XPS) analysis to investigate the electron binding energies of Fe and Co elements in both low-crystalline and high-crystalline samples. As shown in Fig. S4,† the electron binding energy of Fe in the low-crystalline sample is 712.62 eV, which has a 1.34 eV offset compared to that in the high-crystalline sample (711.28 eV). The same trend is also observed in the Co 2p electron binding energy spectra, where the electron binding energy of Co in the low-crystalline state locates at 780.49 eV, which is higher than that in the high-crystalline state (780 eV). These results suggest that the outermost atoms of elements in the amorphous sample are more likely to undergo transitions, which will possibly enhance their electrocatalytic performance.[24,44,45]

To demonstrate its potential as an electrocatalyst, LC-FeCo was tested for the oxygen evolution reaction (OER) and compared to a series of Fe-based (Fig. S5†) and Co-based catalysts (Fig. S6†), as well as commercial RuO_2 serving as the control. In all OER experiments, 1.0 mg of catalysts was deposited on carbon paper with a surface area of 1.0 cm^2 as the working electrode. As shown in Fig. 3a, LC-FeCo exhibited overpotentials of 271 and 352 mV to achieve current densities of 10 and 200 mA cm^{-2}, respectively, and it outperforms HC-FeCo (312 @ and 434 mV @) and commercial RuO_2 (342 mV @ 10 mA cm^{-2}). Additionally, LC-FeCo showed a Tafel slope (Fig. 3b) of 51.6 mV dec^{-1}, which is smaller than those of HC-FeCo (75.5 mV dec^{-1}) and RuO_2 (145.8 mV dec^{-1}), allowing it to generate a higher current density at a lower overpotential. At a potential of 1.60 V, the output current density of LC-FeCo was 276.92 mA cm^{-2}, which was 4.74 times higher than that of commercial HC-FeCo (58.44 mA cm^{-2}) and 17.91 times higher than that of commercial RuO_2 (15.46 mA cm^{-2}). Furthermore, LC-FeCo showed superior catalytic performance compared to pure Fe and Co catalysts (Fig. S7†). Durability is another critical parameter for evaluating electrocatalysts, and LC-FeCo exhibits excellent stability within 20 hours (Fig. 3c), maintaining a stable output current density of 350 mA cm^{-2} at 1.62 V (*vs.* the RHE). At the same operating voltage, highly crystalline FeCo can only obtain a current density of 50 mA cm^{-2}, accompanied by a continuous performance decline. The XPS results indicate that the electron binding energies of Co and Fe both increase to a certain extent after the prolonged reaction (Fig. S8†). The STEM results showed that the tiny aggregates of LC-FeCo existed after prolonged electrolysis, but HR-TEM indicated that the amorphous and crystalline regions still coexisted (Fig. S9†). This suggests that LC-FeCo has the greatest potential to be commercially viable as an OER catalyst (Table S1†).

We hypothesize that the superior OER performance of LC-FeCo can be attributed to its low crystallinity, which enhances the electron/mass transport, and electrochemical active area. To investigate the charge transport kinetics during electrocatalysis, we measured electrical impedance spectra (EIS) in 1.0 M KOH. As seen in Fig. S10,† LC-FeCo exhibited a

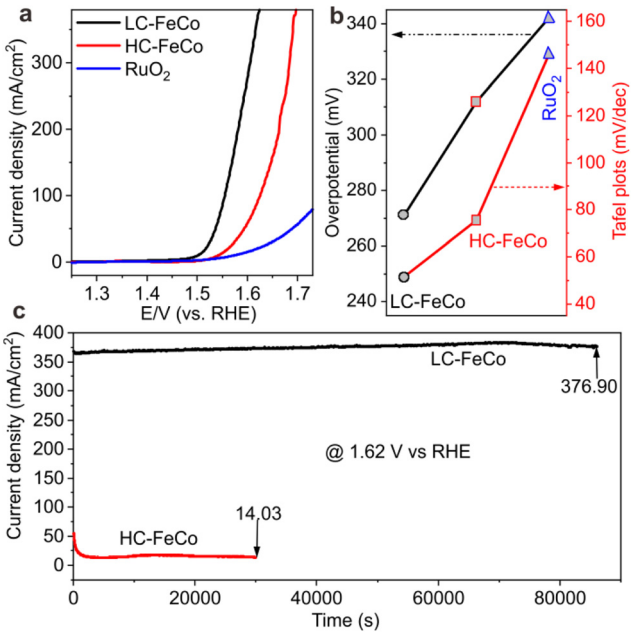

Fig. 3 OER performances of LC-FeCo, HC-FeCo and RuO_2 in KOH. (a) Electrode surface area-normalized polarization curves obtained at a scan rate of 10 mV s^{-1}. (b) Corresponding Tafel plots and the overpotential required for a cathodic current density of 10 mA cm^{-2}. (c) Chronoamperometric curve of LC-FeCo and HC-FeCo at a constant potential of 1.62 V *vs.* RHE. The loading amounts of all catalysts on carbon paper are 1.0 mg cm^{-2}.

lower charge-transfer resistance (4.2 Ω) than HC-FeCo (6.28 Ω), indicating its superior charge transport kinetics.[5,46,47] Furthermore, to identify the intrinsic active sites of the catalyst for the OER, we probed the electrochemical double-layer capacitance (C_{dl}) to estimate the ECSA using cyclic voltammetry scanning in 1.0 M KOH at the scan rates of 10–60 mV s^{-1}. As shown in Fig. S11 and S12,† LC-FeCo showed a significantly larger C_{dl} value (40.3 mF cm^{-2}) than HC-FeCo (30.5 mF cm^{-2}), demonstrating its higher specific surface area and substantial active sites for the OER. Materials with low or non-crystalline structures can endow them with extremely strong self-healing abilities, which enable them to exhibit excellent catalytic stability during electrocatalysis.[7,17,48–50]

It should be noted that LC-FeCo also showed superior HER activity, with an overpotential of 288 mV at a current density of 100 mA cm^{-2}, which is lower than the overpotential required for HC-FeCo (400 mV). At a high outputting current (350 mA cm^{-2}), the performance of LC-FeCo (403 mV) is comparable to that of commercial Pt/C (347 mV) (Fig. S13†). Therefore, the excellent catalytic performance of LC-FeCo in both the HER and OER makes it a promising multifunctional electrocatalyst for overall water splitting. As shown in Fig. 4a, even at a lower output current, LC-FeCo exhibits catalytic activity comparable to precious metals, and LC-FeCo‖LC-FeCo exhibits even better performance. Impressively, at a higher output current, LC-FeCo‖LC-FeCo only requires 1.95 V to achieve 200 mA cm^{-2}, while the reference couple (Pt/C‖IrO_2) requires 2.13 V to achieve the same current density, demonstrating the excellent

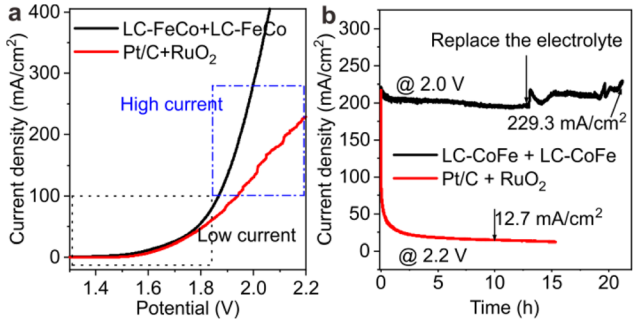

Fig. 4 Water splitting performances of the LC-FeCo + LC-FeCo, and Pt/C + RuO_2 couple in KOH. (a) Electrode surface area-normalized polarization curves obtained at a scan rate of 10 mV s^{-1}. (b) Chronoamperometric curve of the LC-FeCo + LC-FeCo and Pt/C + RuO_2 couple. The loading amounts of all catalysts on carbon paper are 1.0 mg cm^{-2}.

catalytic activity of LC-FeCo-based electrolyzers. Furthermore, LC-FeCo-based electrolyzers also exhibit superior catalytic stability compared to the noble metals. As shown in Fig. 4b, After 20 hours of electrolysis, the output current of 229.3 mA cm^{-2} on the LC-FeCo||LC-FeCo couple can still be maintained, while the durability of Pt/C-IrO_2 is very inferior, with obvious attenuation being observed in the first 5 hours of reaction. After 10 hours of electrolysis, the output current on the Pt/C||RuO_2 couple decreases to 12.7 mA cm^{-2}. These results (Table S2†) suggest that LC-FeCo has great potential to replace precious metals as the next-generation catalysts for electrochemical water splitting under alkaline conditions.

Conclusions

To make nanocatalysts suitable for industrial applications, several factors need to be considered. Firstly, the synthetic cost should be low while ensuring high-quality synthesis on a gram-scale. Secondly, the synthetic process should be simple and safe without the emission of any toxic or harmful substances. Finally, the nanocatalysts should exhibit high catalytic activity and stability. In this study, we have utilized basic inorganic chemistry principles to guide the synthesis and preparation of FeCo catalysts that demonstrate exceptional catalytic activity and stability during overall water splitting. During the anode reaction, Fe and Co species can synergistically function to overcome the potential energy barrier during the oxygen production process. Additionally, the low-crystalline structure of the catalyst further enhances its catalytic activity and stability. Based on the above advantages, LC-FeCo has the potential to replace precious metals as the next generation alkaline water splitting electrolytic cell catalysts.

Author contributions

L. D. proposed the research direction and guided the project. H. R. and C. C. performed the experiments and carried out the electrochemical experiments. H. R., C. C., Q. Q., P. Y. and L. D. analysed and discussed all experimental results and drafted the manuscript. H. R. and C. C. contributed equally to this work. All the authors contributed to the overall scientific interpretation.

Conflicts of interest

There are no conflicts to declare.

Acknowledgements

The authors express their gratitude to the electron microscopy (and/or X-ray) facilities at Henan University, China, provided by the Facility for Analysis, Characterization, Testing, and Simulation. This research received financial support from the National Natural Science Foundation of China (22202059) and the Start-Up Grants from Henan University. Q. Q. gratefully acknowledges financial support from the Start-Up Grants (Project No. 762103) from Anhui Normal University. P. Y. gratefully acknowledges financial support from the Start-Up Grants from Anhui Medical University.

References

1 I. Ledezma-Yanez, W. D. Z. Wallace, P. Sebastián-Pascual, V. Climent, J. M. Feliu and M. T. Koper, *Nat. Energy*, 2017, **2**, 17031.
2 M. Chhetri, S. Sultan and C. Rao, *Proc. Natl. Acad. Sci. U. S. A.*, 2017, **114**, 8986–8990.
3 L. Dai, Z. N. Chen, L. Li, P. Yin, Z. Liu and H. Zhang, *Adv. Mater.*, 2020, **32**, e1906915.
4 M. Gong, W. Zhou, M. C. Tsai, J. Zhou, M. Guan, M. C. Lin, B. Zhang, Y. Hu, D. Y. Wang, J. Yang, S. J. Pennycook, B. J. Hwang and H. Dai, *Nat. Commun.*, 2014, **5**, 4695.
5 Q. Lu, A.-L. Wang, Y. Gong, W. Hao, H. Cheng, J. Chen, B. Li, N. Yang, W. Niu, J. Wang, Y. Yu, X. Zhang, Y. Chen, Z. Fan, X.-J. Wu, J. Chen, J. Luo, S. Li, L. Gu and H. Zhang, *Nat. Chem.*, 2018, **10**, 456–461.
6 H. Wang, H. W. Lee, Y. Deng, Z. Lu, P. C. Hsu, Y. Liu, D. Lin and Y. Cui, *Nat. Commun.*, 2015, **6**, 7261.
7 S. Bai, Y. Mou, J. Wan, Y. Wang, W. Li, H. Zhang, P. Luo and Y. Wang, *Nanoscale*, 2022, **14**, 18123–18132.
8 I. K. Muritala, D. Guban, M. Roeb and C. Sattler, *Int. J. Hydrogen Energy*, 2020, **45**, 26022–26035.
9 M. J. Kenney, M. Gong, Y. Li, J. Z. Wu, J. Feng, M. Lanza and H. Dai, *Science*, 2013, **342**, 836–840.
10 L. Dai, Q. Qin, X. Zhao, C. Xu, C. Hu, S. Mo, Y. O. Wang, S. Lin, Z. Tang and N. Zheng, *ACS Cent. Sci.*, 2016, **2**, 538–544.
11 J. Joo, T. Kim, J. Lee, S. I. Choi and K. Lee, *Adv. Mater.*, 2019, **31**, e1806682.
12 S. Chen, T. Takata and K. Domen, *Nat. Rev. Mater.*, 2017, **2**, 17050.

13 Y. Yang, H. Yao, Z. Yu, S. M. Islam, H. He, M. Yuan, Y. Yue, K. Xu, W. Hao, G. Sun, H. Li, S. Ma, P. Zapol and M. G. Kanatzidis, *J. Am. Chem. Soc.*, 2019, **141**, 10417–10430.
14 Y. Liu, S. Liu, Y. Wang, Q. Zhang, L. Gu, S. Zhao, D. Xu, Y. Li, J. Bao and Z. Dai, *J. Am. Chem. Soc.*, 2018, **140**, 2731–2734.
15 C. Gu, S. Hu, X. Zheng, M. R. Gao, Y. R. Zheng, L. Shi, Q. Gao, X. Zheng, W. Chu, H. B. Yao, J. Zhu and S. H. Yu, *Angew. Chem., Int. Ed.*, 2018, **57**, 4020–4024.
16 X. Wang, Y. V. Kolen'ko, X. Q. Bao, K. Kovnir and L. Liu, *Angew. Chem., Int. Ed.*, 2015, **54**, 8188–8192.
17 C. Cheng, W. Ao, H. Ren, Z. Shen, Z. Fan, T. Xu, W. Liu, Q. Zhang, P. Yin and L. Dai, *Appl. Catal., B*, 2023, **331**, 122681.
18 Z. Zhang, G. Liu, X. Cui, B. Chen, Y. Zhu, Y. Gong, F. Saleem, S. Xi, Y. Du, A. Borgna, Z. Lai, Q. Zhang, B. Li, Y. Zong, Y. Han, L. Gu and H. Zhang, *Adv. Mater.*, 2018, **30**, e1801741.
19 G. Liu, P. Li, G. Zhao, X. Wang, J. Kong, H. Liu, H. Zhang, K. Chang, X. Meng, T. Kako and J. Ye, *J. Am. Chem. Soc.*, 2016, **138**, 9128–9136.
20 Y.-Y. Ma, Z.-L. Lang, L.-K. Yan, Y.-H. Wang, H.-Q. Tan, K. Feng, Y.-J. Xia, J. Zhong, Y. Liu and Z.-H. Kang, *Energy Environ. Sci.*, 2018, **11**, 2114–2123.
21 M. Gao, W. Sheng, Z. Zhuang, Q. Fang, S. Gu, J. Jiang and Y. Yan, *J. Am. Chem. Soc.*, 2014, **136**, 7077–7084.
22 S. Klaus, Y. Cai, M. W. Louie, L. Trotochaud and A. T. Bell, *J. Phys. Chem. C*, 2015, **119**, 7243–7254.
23 H. Sun, X. Xu, H. Kim, W. Jung, W. Zhou and Z. Shao, *Energy Environ. Mater.*, 2023, 12441, DOI: **10.1002/eem2.12441**.
24 C. Cheng, W. Ao, H. Ren, Z. Fan, T. Xu, L. Dai and P. Yin, *Sci. China Mater.*, 2023, **66**, 1383–1388.
25 Y. P. Zhu, C. Guo, Y. Zheng and S.-Z. Qiao, *Acc. Chem. Res.*, 2017, **50**, 915–923.
26 J. Chen, G. Liu, Y. Z. Zhu, M. Su, P. Yin, X. J. Wu, Q. Lu, C. Tan, M. Zhao, Z. Liu, W. Yang, H. Li, G. H. Nam, L. Zhang, Z. Chen, X. Huang, P. M. Radjenovic, W. Huang, Z. Q. Tian, J. F. Li and H. Zhang, *J. Am. Chem. Soc.*, 2020, **142**, 7161–7167.
27 Z. Zhang, G. Liu, X. Cui, Y. Gong, D. Yi, Q. Zhang, C. Zhu, F. Saleem, B. Chen and Z. Lai, *Sci. Adv.*, 2021, **7**, eabd6647.
28 F. Hu, D. Yu, M. Ye, H. Wang, Y. Hao, L. Wang, L. Li, X. Han and S. Peng, *Adv. Energy Mater.*, 2022, **12**, 2200067.
29 K. Wang, Y. Guo, Z. Chen, D. Wu, S. Zhang, B. Yang and J. Zhang, *InfoMat*, 2021, **4**, e12251.
30 H. Xie, D. Jiang, H. Chen, X. Ma, X. Liu, Q. Qi and Y. Wang, *Nanoscale*, 2023, **15**, 7430–7437.
31 W. Yu, Z. Chen, Y. Zhao, Y. Gao, W. Xiao, B. Dong, Z. Wu and L. Wang, *Nanoscale*, 2022, **14**, 4566–4572.
32 X. Zhu, C. Tang, H.-F. Wang, B.-Q. Li, Q. Zhang, C. Li, C. Yang and F. Wei, *J. Mater. Chem. A*, 2016, **4**, 7245–7250.
33 M. Chen, D. Liu, B. Zi, Y. Chen, D. Liu, X. Du, F. Li, P. Zhou, Y. Ke, J. Li, K. H. Lo, C. T. Kwok, W. F. Ip, S. Chen, S. Wang, Q. Liu and H. Pan, *J. Energy Chem.*, 2022, **65**, 405–414.
34 Y. Pan, M. Wang, M. Li, G. Sun, Y. Chen, Y. Liu, W. Zhu and B. Wang, *J. Energy Chem.*, 2022, **68**, 699–708.
35 X. Lu and C. Zhao, *Nat. Commun.*, 2015, **6**, 6616.
36 P. Babar, K. Patil, J. Mahmood, S.-J. Kim, J. H. Kim and C. T. Yavuz, *Cell Rep. Phys. Sci.*, 2022, **3**, 100762.
37 C. Hu, Q. Ma, S.-F. Hung, Z.-N. Chen, D. Ou, B. Ren, H. M. Chen, G. Fu and N. Zheng, *Chem*, 2017, **3**, 122–133.
38 Y. Liu, C. Xiao, P. Huang, M. Cheng and Y. Xie, *Chem*, 2018, **4**, 1263–1283.
39 D. P. Sahoo, K. K. Das, S. Mansingh, S. Sultana and K. Parida, *Coord. Chem. Rev.*, 2022, **469**, 214666.
40 T. Kwon, M. Jun, J. Joo and K. Lee, *J. Mater. Chem. A*, 2019, **7**, 5090–5110.
41 S. Liu, S. Geng, L. Li, Y. Zhang, G. Ren, B. Huang, Z. Hu, J. F. Lee, Y. H. Lai, Y. H. Chu, Y. Xu, Q. Shao and X. Huang, *Nat. Commun.*, 2022, **13**, 1187.
42 Z. Zheng, L. Lin, S. Mo, D. Ou, J. Tao, R. Qin, X. Fang and N. Zheng, *Small*, 2018, **14**, 1800759.
43 Z. Liu, K. Nie, X. Qu, X. Li, B. Li, Y. Yuan, S. Chong, P. Liu, Y. Li, Z. Yin and W. Huang, *J. Am. Chem. Soc.*, 2022, **144**, 4863–4873.
44 L. Yang, R. Liu and L. Jiao, *Adv. Funct. Mater.*, 2020, **30**, 1909618.
45 H. Huang, A. Cho, S. Kim, H. Jun, A. Lee, J. W. Han and J. Lee, *Adv. Funct. Mater.*, 2020, **30**, 2003889.
46 S. Gao, Y. Lin, X. Jiao, Y. Sun, Q. Luo, W. Zhang, D. Li, J. Yang and Y. Xie, *Nature*, 2016, **529**, 68.
47 L. Dai, Q. Qin, P. Wang, X. Zhao, C. Hu, P. Liu, R. Qin, M. Chen, D. Ou, C. Xu, S. Mo, G. Fu, P. Zhang and N. Zheng, *Sci. Adv.*, 2017, **3**, e1701069.
48 Y. Yang, K. Zhang, H. Lin, X. Li, H. C. Chan, L. Yang and Q. Gao, *ACS Catal.*, 2017, **7**, 2357–2366.
49 Y. Zeng, M. Zhao, Z. Huang, W. Zhu, J. Zheng, Q. Jiang, Z. Wang and H. Liang, *Adv. Energy Mater.*, 2022, **12**, 2201713.
50 G.-F. Chen, T. Y. Ma, Z.-Q. Liu, N. Li, Y.-Z. Su, K. Davey and S.-Z. Qiao, *Adv. Funct. Mater.*, 2016, **26**, 3314–3323.